

UNCLASSIFIED

SECURITY CLASSIFICATION OF THIS PAGE

REPORT DOCUMENTATION PAGE

Form Approved
OMB No. 0704-0188

1a. REPORT SECURITY CLASSIFICATION
Unclassified

1b. RESTRICTIVE MARKINGS
None

DTIC FILE COPY

2. ABSTRACT SECURITY CLASSIFICATION

3. DISTRIBUTION / AVAILABILITY OF REPORT
Approved for public release;
distribution unlimited

AD-A205 002

5. MONITORING ORGANIZATION REPORT NUMBER(S)

6a. NAME OF PERFORMING ORGANIZATION
Coordinated Science Lab
University of Illinois

6b. OFFICE SYMBOL
(If applicable)
N/A

7a. NAME OF MONITORING ORGANIZATION
Office of Naval Research

6c. ADDRESS (City, State, and ZIP Code)
1101 W. Springfield Ave.
Urbana, IL 61801

7b. ADDRESS (City, State, and ZIP Code)
800 Quincy St.
Arlington, VA 22217

8a. NAME OF FUNDING / SPONSORING ORGANIZATION
SDIO

8b. OFFICE SYMBOL
(If applicable)
IST

9. PROCUREMENT INSTRUMENT IDENTIFICATION NUMBER
ONR N00014-86-K-0513

8c. ADDRESS (City, State, and ZIP Code)
800 Quincy St.
Arlington, VA 22217

10. SOURCE OF FUNDING NUMBERS

PROGRAM ELEMENT NO.	PROJECT NO.	TASK NO.	WORK UNIT ACCESSION NO.
63221C	s400	05	01

11. TITLE (Include Security Classification)

Novel High Speed Devices and Heterostructures Prepared by Molecular Beam Epitaxy

12. PERSONAL AUTHOR(S)

Professor Hadis Morkoç

13a. TYPE OF REPORT
Progress

13b. TIME COVERED
FROM 10/87 TO 9/88

14. DATE OF REPORT (Year, Month, Day)
February 13, 1989

15. PAGE COUNT

16. SUPPLEMENTARY NOTATION

17. COSATI CODES

FIELD	GROUP	SUB-GROUP

18. SUBJECT TERMS (Continue on reverse if necessary and identify by block number)

19. ABSTRACT (Continue on reverse if necessary and identify by block number)

Please see section entitled, "Summary"

DTIC
ELECTE
S FEB 22 1989 D
D CS D

20. DISTRIBUTION / AVAILABILITY OF ABSTRACT
 UNCLASSIFIED UNLIMITED SAME AS RPT. DTIC USERS

21. ABSTRACT SECURITY CLASSIFICATION
Unclassified

22a. NAME OF RESPONSIBLE INDIVIDUAL
Prof. H. Morkoç

22b. TELEPHONE (Include Area Code)
217-333-9736

22c. OFFICE SYMBOL

TABLE OF CONTENTS

1. Summary	1
2. Progress Made	3
3. Publications/Presentations/Honors	20



Accession For	
NTIS CRA&I	<input checked="" type="checkbox"/>
DTIC TAB	<input type="checkbox"/>
Unannounced	<input type="checkbox"/>
Justification _____	
By _____	
Distribution /	
Availability Codes	
Dist	Avail and/or Special
A-1	

1. Summary

Study of the small-bandgap III-V compounds $\text{InAs}_{1-x}\text{Sb}_x$ and $\text{GaAs}_{1-x}\text{Sb}_x$ has continued towards the goal of eventual application to long wavelength infrared sources and detectors, in this last year of our current research contract sponsored by SDIO/IST Electronic/Optical Materials.

Optical characterization of these small bandgap compounds was performed, resulting in the best reported low-temperature photoluminescence linewidth of 7.6 meV for a $\text{GaAs}_{0.49}\text{Sb}_{0.51}$ sample.

Additionally, the first experimental data on the band alignment of the GaSb/GaAs system was reported from the results of photoreflectance measurements: we reported a heavy-hole band offset

of 1.7 eV for $\text{GaAs}_{0.9}\text{Sb}_{0.1}$, establishing a type-II structure with electrons in the GaAs layers and holes in the $\text{GaAs}_{1-x}\text{Sb}_x$ layers. Electrical characterization of these materials was also studied by variable temperature Hall measurements. For the $\text{GaAs}_{1-x}\text{Sb}_x$ material grown on InP, a two-acceptor model was forwarded to describe the Hall coefficient temperature behavior.

More directly addressing the goal of optoelectronic integration, we have investigated the growth of these materials lattice mismatched to both GaAs and Si substrates. In studying the growth of $\text{InAs}_{1-x}\text{Sb}_x$ on GaAs, we have reported the effects of using graded layers, strained-layer superlattices, and tilted substrates to reduce or constrain the misfit dislocations induced by the large lattice mismatch (7.2 - 14.6% for $0 \leq x \leq 1$). Transmission electron microscopy on the microstructure and interfacial structure of the InSb layers on (100) GaAs has revealed the accommodation of the misfit strain by square arrays of $a/2[011]$ edge-type dislocations. We have presented a model to explain the formation of these dislocation arrays. Meanwhile, from Hall measurements, room temperature electron mobilities as high as $57000 \text{ cm}^2/\text{V}\cdot\text{s}$ were reported in a $4.6 \mu\text{m}$ thick unintentionally-doped InSb layer on GaAs. For a $1.6 \mu\text{m}$ thick $\text{InAs}_{1-x}\text{Sb}_x$ ($x = 0.67$) layer, electron mobilities of 20000 and $8800 \text{ cm}^2/\text{V}\cdot\text{s}$ were reported at 300 and 77 K, respectively.

The growth of both InAs and InSb epilayers on (100) Si substrates tilted 4° towards (110) was pursued despite the 11.3% and 19% lattice mismatches between the epilayer and substrate materials. X-ray rocking curve measurements and optical transmission measurements were performed

to determine the structural and optical properties of the epilayers. From Hall measurements, room temperature electron mobilities as high as $55000 \text{ cm}^2/\text{V}\cdot\text{s}$ were realized in a thick $8 \text{ }\mu\text{m}$ InSb epilayer. For the InAs epilayers, a peak electron mobility of $45000 \text{ cm}^2/\text{V}\cdot\text{s}$ was reported for a thick $6.7 \text{ }\mu\text{m}$ film at 75 K.

A significant breakthrough has been achieved in the fabrication of hot-electron transistors (HET) through our development of the contact regrowth (CORE) technique for the formation of extremely low-resistance nonalloyed ohmic contacts. The potential of our CORE structure for improving device performance and uniformity suggests a wide variety of applications in the processing of semiconductor devices. In our report, the CORE structure was investigated for achieving low-resistance nonalloyed contacts to the thin base of the HET. Although a relatively thicker (for a HET device) 1000 \AA $\text{In}_{0.53}\text{Ga}_{0.47}\text{As}$ base layer was used in the initial investigation, a very low specific contact resistance of $1.8 \times 10^{-7} \text{ }\Omega\cdot\text{cm}^2$ of the nonalloyed base contact was reported. While the thicker base structure of the HET gave expectedly low transfer ratios, excellent performance of the low-resistance contacts was reported. The development of the CORE technique addresses some of the current limitations in the HET device: higher current densities may now be realized through the uniform, low-resistance base contact. Further, vertical scaling of the base epitaxial layer may also proceed, which should lead to improved transfer ratios.

Preliminary investigation of the microstructure and interfacial structure of the CORE structure has commenced, towards the optimization of the regrowth process for device application. We include yet unreported cross-sectional TEM analyses of the CORE structure. Finally, concurrent theoretical calculations have also been pursued. The calculation of the I-V characteristics of direct tunneling diodes describes the injection of electrons through the HET emitter-base tunneling barrier. Our unique simulation approach reports the first known quantitative agreement of calculated tunneling current with experiment.

2. Progress Made

GaAs_{1-x}Sb_x Films

In our studies on GaAs_{1-x}Sb_x alloys, we have reported both optical and electrical characteristics of this material grown on GaAs and InP substrates. Investigating the broadening effects of the observed microstructural nonuniformities on the optical properties of this material, low temperature (4 K) photoluminescence (PL) was performed. For samples with $x < 0.06$, PL spectra were dominated by two bands, as shown in Fig. 1 for a sample with $x = 0.044$, under varying laser excitation intensities. The narrow peak at higher energy is attributed to the emission associated with the annihilation of excitons bound to impurities (BE), whereas the broad peak at lower energy is attributed to the recombination of electrons in the conduction band (e,A), as well as electrons bound to donors (D,A) with holes bound to acceptors. When the low excitation intensities are used (Fig. 1a), the acceptor bound excitons are more pronounced and have lower peak energy. At higher pump intensity (Fig. 1b), the acceptor bound excitons quickly saturate, with the donor bound exciton completely dominating at even stronger excitation (Fig. 1c). To verify our assignments of PL peaks, we also performed transmission measurements where the free exciton transitions dominate. A strong exciton (ground) peak was observed as well as a weak dip at higher energy, which is attributed to the absorption due to free excitons in the excited state.

For $x > 0.06$, only one peak associated with the impurity or defect related transition dominates PL spectra. In the range $0.1 \leq x \leq 0.3$, the full width at half maximum (FWHM) of the dominant peak is generally < 25 meV, with very little variation. For lattice-mismatched films with $x > 0.3$, the luminescence becomes quite broad and very weak, due at least in part to the high density of dislocations inherent in these films. In contrast, layers grown nearly lattice matched ($0.45 \leq x \leq 0.54$) to InP substrates display good PL spectra. A single emission peak is typically observed at 0.780–0.790 eV with FWHM ≤ 12 meV. A best reported peak width of 7.6 meV is presented in Fig. 2 for a GaAs_{0.46}Sb_{0.54} sample.

Low temperature optical absorption measurements were performed to directly measure the bandgap of this material. Extrapolation of absorption coefficient squared (α^2) versus energy plots

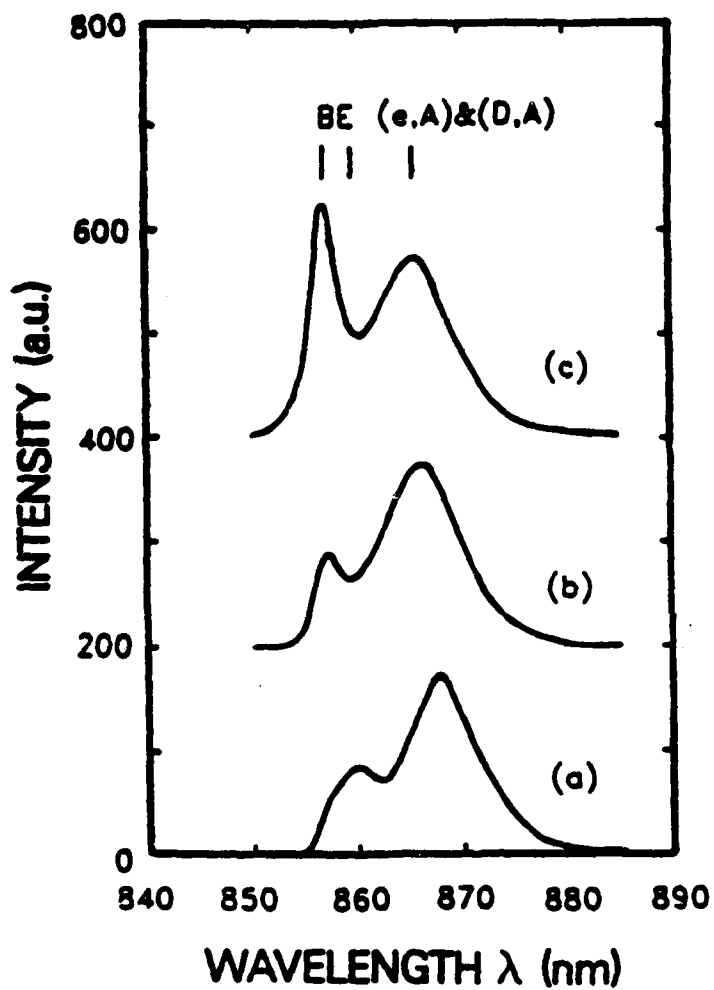


Fig. 1 Normalized PL spectra of a GaAs_{1-x}Sb_x ($x = 0.044$) film under varying laser intensities: a) 2 W/cm²; b) 20 W/cm²; c) 200 W/cm².

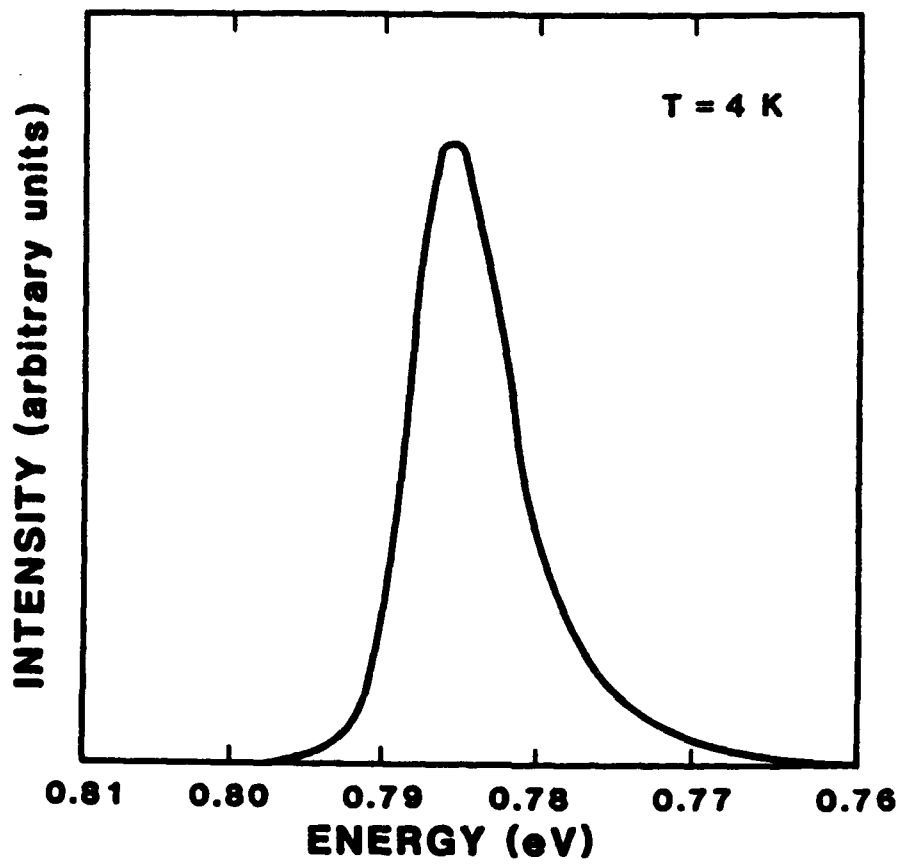


Fig. 2 Low temperature PL spectrum of a $\text{GaAs}_{0.46}\text{Sb}_{0.54}$ film displaying the narrowest peak reported to date.

to $\alpha^2 = 0$ shows a bandgap of 0.804 eV at 4 K and 0.722 eV at 300 K for $\text{GaAs}_{0.5}\text{Sb}_{0.5}$, consistent with our PL data. Fig. 3 shows E_g versus x at 300 K found by similar absorption measurements for a large number of $\text{GaAs}_{1-x}\text{Sb}_x$ samples grown both on GaAs and InP substrates. The E_g values plotted in Fig. 3 are possibly overestimated due to biaxial compression of the lattice from the positive mismatch with the substrate; however, this effect was minimized by growing relatively thick 1.0–3.0 μm layers. Fitting our data, we reported the bandgap energy relation

$$E_g = 1.42 - 2.05x + 1.35x^2,$$

shown as a dashed line in Fig. 3. The solid line plotted in Fig. 3 is the previously accepted relation suggested by Nahory et al.

$\text{GaAs}_{1-x}\text{Sb}_x$ films grown on Fe-doped InP substrates were characterized by variable temperature Hall measurements. Advancing a two-acceptor model, a good fit to the Hall coefficient versus temperature behavior was reported in the temperature range $30 \text{ K} < T < 300 \text{ K}$. Low hole mobilities $< 200 \text{ cm}^2/\text{V}\cdot\text{s}$ for $T < 300 \text{ K}$ are consistent with previous observations. A simple alloy cluster scattering model has been shown to be useful in explaining the mobility versus temperature characteristics.

GaAs_{1-x}Sb_x/GaAs SLSs

The growth of high quality $\text{GaAs}_{1-x}\text{Sb}_x/\text{GaAs}$ strained-layer superlattices (SLSs) and their characterization by TEM have previously been reported in conjunction with this research project. In our current efforts, we have further characterized the $\text{GaAs}_{1-x}\text{Sb}_x/\text{GaAs}$ superlattice by x-ray diffraction to accurately determine the structural parameters of the superlattices. Additionally, low temperature and room temperature photorefectance (PR) measurements were performed for the evaluation of band discontinuities resulting in the first experimental report on the band alignment of the GaSb/GaAs system.

Shown in Fig. 4 is a characteristic photorefectance spectrum for a sample at 80 K. This spectrum exhibits a single peak at the low-energy end of the spectrum (1), an intermediate region containing several smaller peaks (2), and a strong double peak at the high energy end

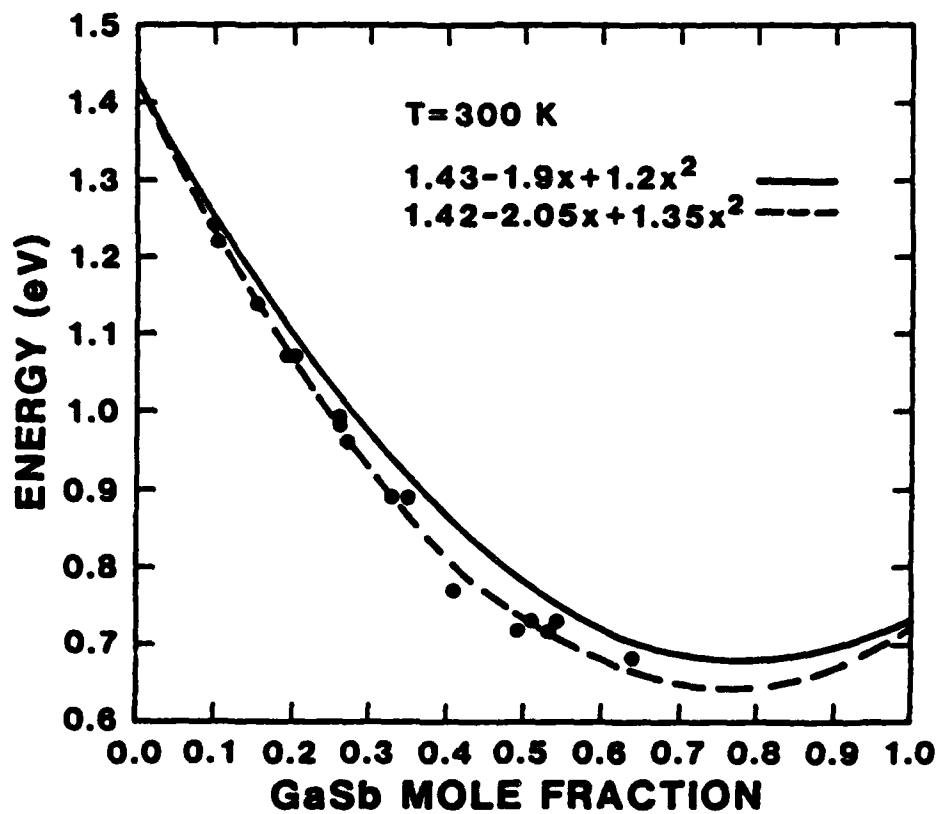


Fig. 3 Room temperature bandgap versus composition for $\text{GaAs}_{1-x}\text{Sb}_x$ layers as measured by optical absorption.

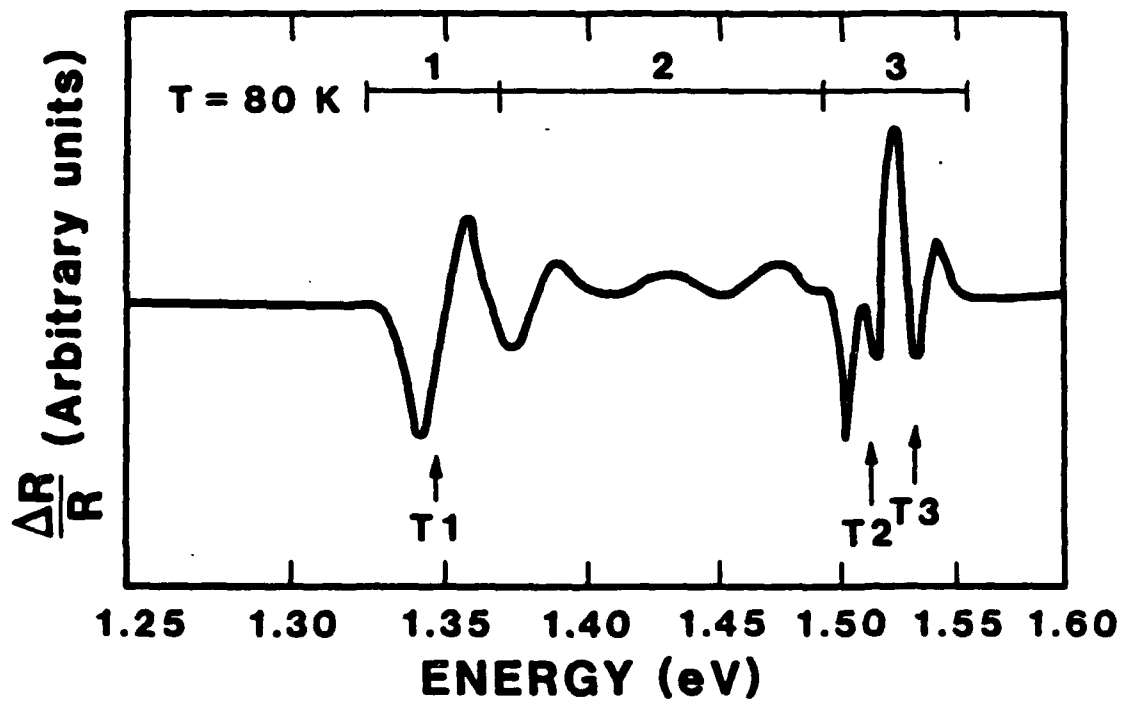


Fig. 4 PR spectrum for a $\text{GaAs}_{1-x}\text{Sb}_x/\text{GaAs}$ superlattice sample at 80 K.

(3). The T1 feature is assigned the lowest energy transition from the $n=1$ heavy hole to $n=1$ conduction band state (1H-1C). Since splitting of the T2 and T3 features cannot be accounted for assuming a Type I superlattice, we proposed a Type II superlattice with electrons in the GaAs layers and holes in the $\text{GaAs}_{1-x}\text{Sb}_x$ layers. The T3 feature then corresponds to a transition between continuum states, and the transition T2 is between a valence band continuum state and the $n = 1$ confined conduction band state. A good fit of the measured and calculated transition energies suggests a heavy-hole band offset value ≈ 1.7 for $\text{GaAs}_{1-x}\text{Sb}_x/\text{GaAs}$ with $x = 0.1$.

InAs_{1-x}Sb_x Films

In our studies of small-bandgap III-V compounds, we have recently investigated the growth and characterization of InSb and its alloy $\text{InAs}_{1-x}\text{Sb}_x$. We have reported on the growth of $\text{InAs}_{1-x}\text{Sb}_x$ on (100) GaAs substrates as well as on (100) Si substrates tilted 4° towards (110) by MBE. Growth of InSb on (100) GaAs was performed over a wide range of conditions including varying substrate temperatures from 330 to 410 °C and Sb/In flux ratios, as well as both 4° and 7° substrate tilt towards (111)A. For an Sb/In flux ratio ~ 1 and a substrate temperature of 540 °C, remarkably good morphologies were reported for InSb on untilted GaAs substrates. Meanwhile, a reduced sensitivity of the $\text{InAs}_{1-x}\text{Sb}_x$ alloy to the growth temperature was observed.

We have examined the microstructure and interfacial structure of InSb films grown on (100) GaAs using transmission electron microscopy (TEM). Shown in Fig. 5 is a selected area diffraction pattern of a $5 \mu\text{m}^2$ area along the (100) direction. In addition to the square InSb(100) diffraction pattern, a square GaAs(100) pattern is also observed from the undiffracted incident beam as well as the beams diffracted from the InSb layer. Measurement of the splitting between pairs of reflections yields a lattice mismatch of 14.6%, in agreement with the bulk lattice parameters. Figure 6 shows an axial (011) lattice image of the interfacial region. The lattice mismatch between film and substrate shows accommodation of the misfit strain by square arrays of $a/2\{0\bar{1}1\}$ edge-type misfit dislocations spaced on average 29 Å apart. We have proposed a model for the formation of these dislocation arrays in which we envision dislocation formation occurring when the lateral growth of InSb islands exceed ~ 30 Å along a given [011] direction.

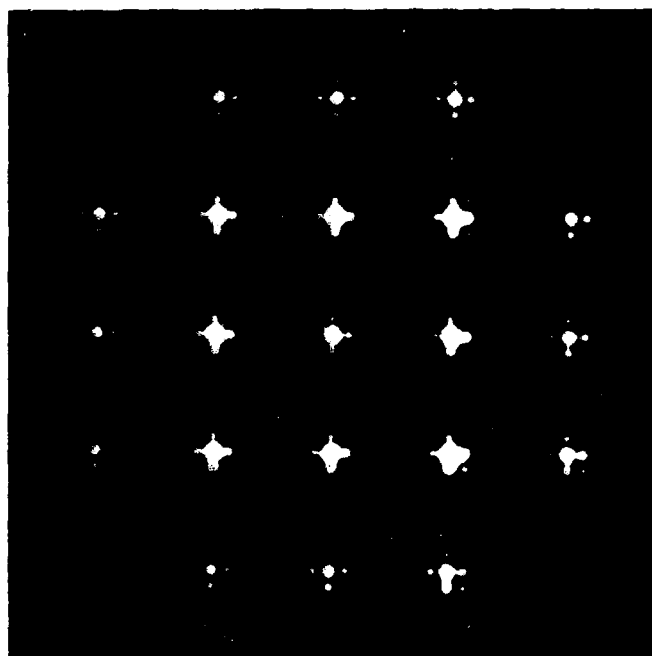


Fig. 5 Selected area diffraction pattern of an InSb epilayer on (100) GaAs along the (100) bicrystal axis.



Fig. 6 Axial (011) high resolution electron micrograph of the InSb/GaAs interface. A misfit dislocation occurs in each bright region along the interface.

Room temperature and 77 K Hall measurements were performed to assess the electrical quality of the InSb epilayers. Carrier concentration and electron mobility were found to be strong functions of layer thickness. For a 5 μm thick epilayer, room temperature mobilities as high as 57000 $\text{cm}^2/\text{V}\cdot\text{s}$ were measured with $N_D - N_A \sim 1.6 \times 10^{16} \text{ cm}^{-3}$. At lower temperatures, however, a rapid decrease in mobility was observed, which is attributed to an increasing dominance of dislocation scattering. The first electrical properties of $\text{InAs}_{1-x}\text{Sb}_x$ ($0.4 < x < 0.7$) epilayers on GaAs substrates was also reported. For a 1.6 μm thick $\text{InAs}_{0.33}\text{Sb}_{0.67}$ layer on GaAs with a 1 μm InSb buffer, electron mobilities of 20000 and 8800 $\text{cm}^2/\text{V}\cdot\text{s}$ were measured at 300 K and 77 K, respectively.

Growth of InSb directly on a Si substrate (tilted 4° off (100) towards (110)) as well as with a GaAs buffer was also reported. Although surface morphologies of the InSb layers grown with and without a GaAs buffer layer look similar, the electrical properties obtained from Hall effect measurements revealed significant differences, especially at 77 K. Room temperature mobilities of 48000 and 39000 $\text{cm}^2/\text{V}\cdot\text{s}$ were measured for 3.2 μm thick layers with and without a 0.3 μm GaAs buffer, respectively. For a thicker 8 μm InSb layer, an electron mobility of 55000 $\text{cm}^2/\text{V}\cdot\text{s}$ was reported. This is consistent with x-ray rocking curve measurements, which show a reduction in FWHM from 600 to 400 arc-seconds for the 3.2 and 8 μm thick InSb films. Similarly, the sharpest band edge transmission spectra is observed for the thick 8 μm InSb film. Finally, a 40 meV shift towards lower energy is reported for the low temperature PL peak of InSb on Si, as compared to bulk InSb.

InAs Films

Optimum growth conditions of InAs epilayers on GaAs has been studied leading to the recent investigation and subsequent report of the first growth of InAs epitaxial films on Si substrates by MBE. InAs epilayers with thicknesses ranging 0.5 to 7.0 μm were grown on (100) GaAs substrates, tilted 7° towards (111)A, and tilted 4° towards (001). Using substrate temperature control, As-stabilized (370-500 °C) and In-stabilized (> 500 °C) growth conditions were studied as well as In-stabilized nucleation with As-stabilized growth: The In-stabilized condition displayed the

smoother surface morphologies. From Hall measurements, thickness dependent electron mobilities from $1.5\text{--}5.2 \times 10^4 \text{ cm}^2/\text{V}\cdot\text{s}$ were measured for $1.0\text{--}6.2 \mu\text{m}$ thick InAs epilayers at 77 K.

The growth of InAs on Si was studied for film thicknesses ranging from 4.0 to $7.0 \mu\text{m}$. Preceded by a thin ($< 0.1 \mu\text{m}$) buffer layer of GaAs and a five-period $\text{In}_{0.8}\text{Ga}_{0.2}\text{As}/\text{GaAs}$ SLS under As-rich conditions, growth of the InAs was performed under In-stabilized conditions at substrate temperatures between 520 and $550 \text{ }^\circ\text{C}$. A maximum electron mobility of $4.5 \times 10^4 \text{ cm}^2/\text{V}\cdot\text{s}$ was reported at 77 K.

InGaAs/InAlAs Hot Electron Transistor

In our continuing studies on the InGaAs/InAlAs hot electron transistor (HET), we have achieved a significant breakthrough in the fabrication of these devices by developing the novel contact regrowth (CORE) technique for the formation of extremely low nonalloyed ohmic contacts. In our previous reports, we have presented improved current gains through vertical scaling of the base epitaxial layer. While further vertical scaling of the HET poses few problems in terms of MBE growth, reliable fabrication of transistor devices becomes increasingly difficult, particularly in the formation of low-resistance ohmic contacts to a base transit region of the order of 100 \AA . The thermal cycling typical of conventional contact formation not only results in non-uniformity and irreproducibility of the contacts, but it can also short the thin base layer.

In our associated studies on the growth of $\text{In}_x\text{Ga}_{1-x}\text{As}$ and $\text{In}_y\text{Al}_{1-y}\text{As}$, we have reported on the use of n^+ -InAs cap layers for low-resistance nonalloyed ohmic contacts to InGaAs. Employing n^+ -InAs/ $\text{In}_{0.53}\text{Ga}_{0.47}\text{As}$ SLSs, we have further reported nonalloyed resistances of less than $1.5 \times 10^{-8} \Omega\cdot\text{cm}^2$ on $\text{In}_{0.53}\text{Ga}_{0.47}\text{As}$. We have successfully applied this in-situ grown structure on heterojunction bipolar transistors. Extending this contacting structure as a regrowth procedure, we have reported the Contact Regrowth (CORE) technique for achieving low-resistance ($1.8 \times 10^{-7} \Omega\cdot\text{cm}^2$) non-alloyed contacts to the base of the HET.

In our published report, an InGaAs/InAlAs HET with a thicker 1000 \AA base layer was investigated. A control HET sample was processed conventionally alongside a second (CORE) sample, which was processed for subsequent MBE regrowth of the InAs contact structure. After

definition of emitter, base and collector mesas by wet chemical etching, the CORE sample was cleaned and loaded into the MBE system, where the following CORE structure was grown: a 30 Å $\text{In}_{0.53}\text{Ga}_{0.47}\text{As}$ layer Si-doped $1.5 \times 10^{18} \text{ cm}^{-3}$; an 8 period 10 Å InAs/10 Å GaAs SLS Si-doped $3 \times 10^{18} \text{ cm}^{-3}$; and finally a 100 Å InAs cap layer Si-doped $3 \times 10^{18} \text{ cm}^{-3}$. Processing of the CORE sample was then completed by evaporation of metal contacts.

The emitter current versus emitter-base bias for both the control and CORE samples with nonalloyed contacts are shown in Fig. 7. The current levels measured in the CORE sample are in general agreement with predicted tunneling currents reflecting the low parasitic resistance achieved by the CORE structure. In contrast, large and highly nonuniform emitter and base contact resistances were measured for the conventional HET devices. Collector current and transconductance versus collector-base bias curves are shown in Fig. 8 for the CORE sample. As expected, with the 1020 Å base plus 500 Å analyzer barrier, a low maximum α of only 0.5 was measured. However, clear voltage shifts in the ballistic peaks were resolved (not obscured by large series resistances) from which a collector barrier height of 450 meV was estimated, in reasonable agreement with thermionic emission measurements.

The development of contact regrowth for the HET suggests the eventual realization of devices with ultra-thin base layers (~ 100 Å), with the associated achievement of "useful" transfer ratios. Furthermore, the higher current densities measured with the CORE structure addresses one of the present limitations of the HET device. Additionally, the self-aligned nature of the regrown contact layer relaxes the demanding requirements of photolithographic processes. Recently, we have pursued a detailed investigation of the CORE structure in order to fully characterize the growth conditions and the resultant layer morphology and electrical properties. Optimization of the CORE procedure for uniform two-dimensional growth and suppression of possible sidewall growth is currently underway, in collaboration with Prof. F. Tsen and co-workers at Arizona State University. Shown in Fig. 9 is a TEM micrograph of a CORE-structure/in-situ-epilayer interface.

Meanwhile, in conjunction with our experimental studies, we have performed calculations of the I-V characteristics of direct tunneling diodes, simulating the carrier injection through the

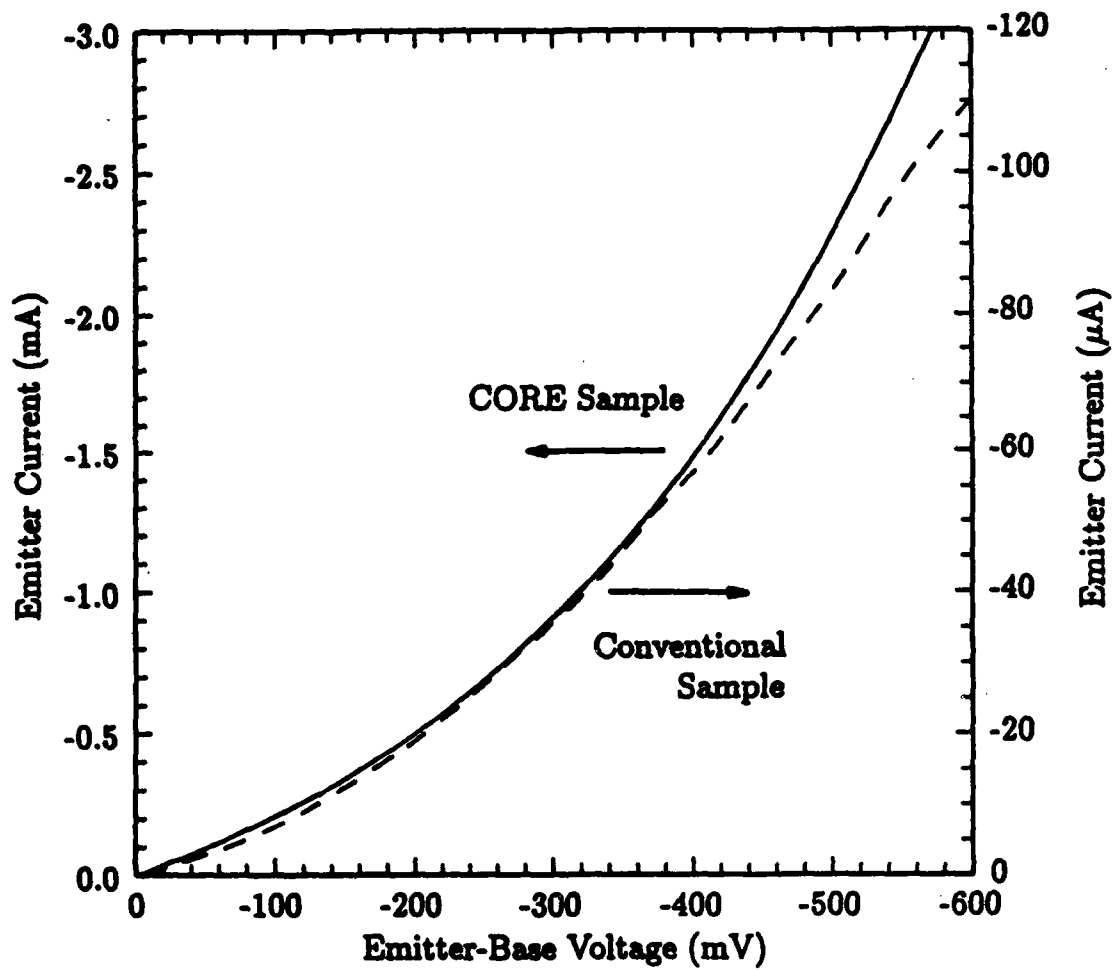


Fig. 7 Emitter current versus emitter-base bias for the HET device both with and without the CORE structure.

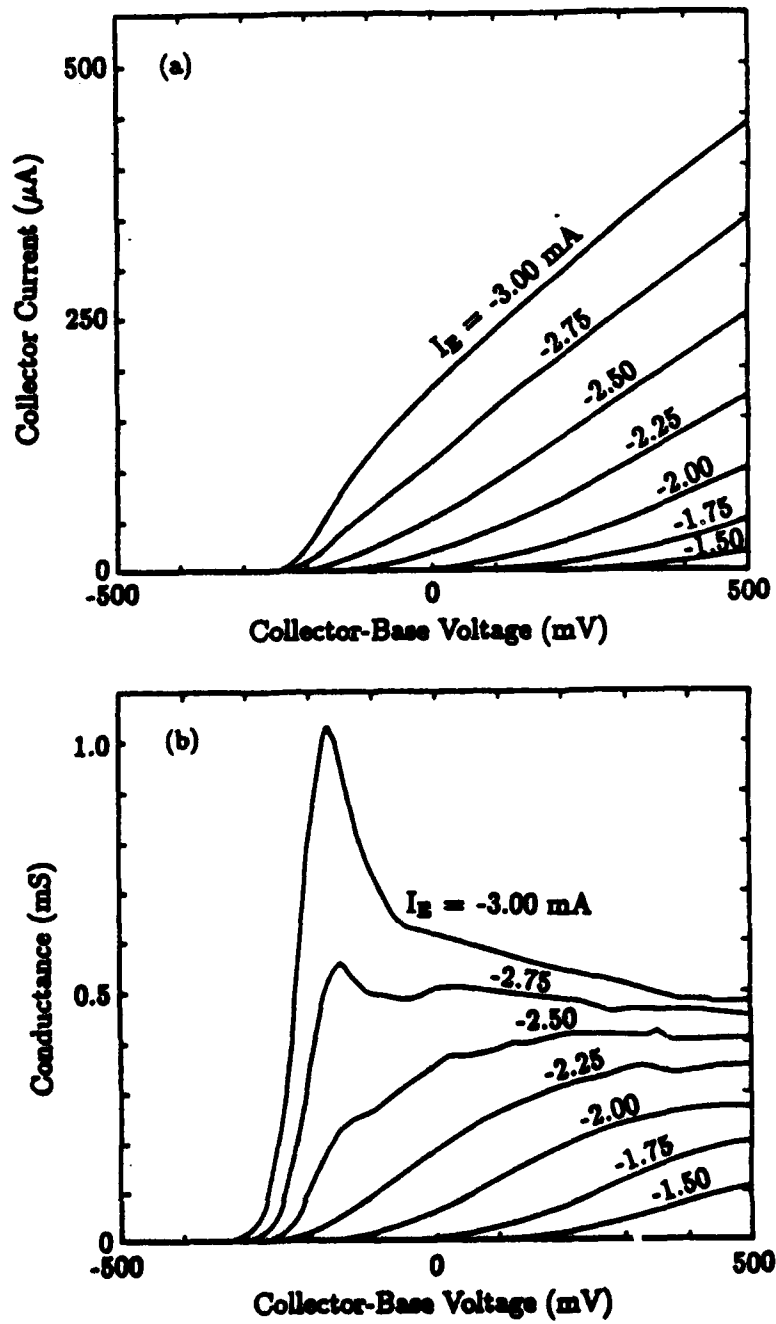


Fig. 8 a) Collector current and b) conductance versus collector-base bias for the CORE HET sample.

Fig. 9 Cross-sectional TEM image of the CORE/*in-situ* In_{0.53}Ga_{0.47}As structure.

emitter-base tunneling barrier. Although several numerical simulations have been done in the past on the I-V characteristics of the tunneling diode, our results report the first quantitative agreement between calculations and experimental results. To obtain quantitative agreement with experiment, 1) the effect of band-bending in the space-charge regions was included by solving two coupled one-dimensional Poisson's equations, and 2) the transmission probability of the tunneling electron was calculated by a transfer matrix method, with the complex k-vector determined by k-p band structure calculations.

We report forward and reverse tunneling current density relations, closely fitting the observed tunneling current:

$$j_F = \frac{qm_0m^*k_B T}{2\pi^2\hbar^3} \left(\frac{1}{1 - e^{(-V_s/k_B T)}} \right) \int_0^\infty |T_F(E_z)|^2 \left[\ln \left(\frac{1 + e^{((V_1(-\infty)+V_{b_l}-E_z)/k_B T)}}{1 + e^{((V_2(\infty)-V_i-V_{b_r}-E_z)/k_B T)}} \right) \right] dE_z,$$

$$j_R = \frac{qm_0m^*k_B T}{2\pi^2\hbar^3} \left(\frac{1}{1 - e^{(V_s/k_B T)}} \right) \int_0^\infty |T_R(E_z)|^2 \left[\ln \left(\frac{1 + e^{((V_2(\infty)+V_{b_r}-E_z)/k_B T)}}{1 + e^{((V_1(-\infty)+V_i+V_{b_l}-E_z)/k_B T)}} \right) \right] dE_z,$$

where V_s is the applied voltage, T_F and T_R are the forward and backward tunneling amplitude, E_z is the energy in the z-direction, V_{b_l} and V_{b_r} represent the band-bending at the left and right terminals, V_i is the voltage drop across the tunneling barrier, and the Fermi energy subscripts 1 and 2 correspond to the left and right terminals. Details of the calculations and the resultant relations are presented in our paper. For a 76 Å i-In_{0.52}Al_{0.48}As barrier bounded by asymmetrically doped n⁺-In_{0.53}Ga_{0.47}As, I-V characteristics were computed and compared to experimentally measured values. Our calculations (short dashed line) and experimental results (solid line) are presented in Fig. 10 along with calculations by conventional effective-mass approximation (long dashed line).

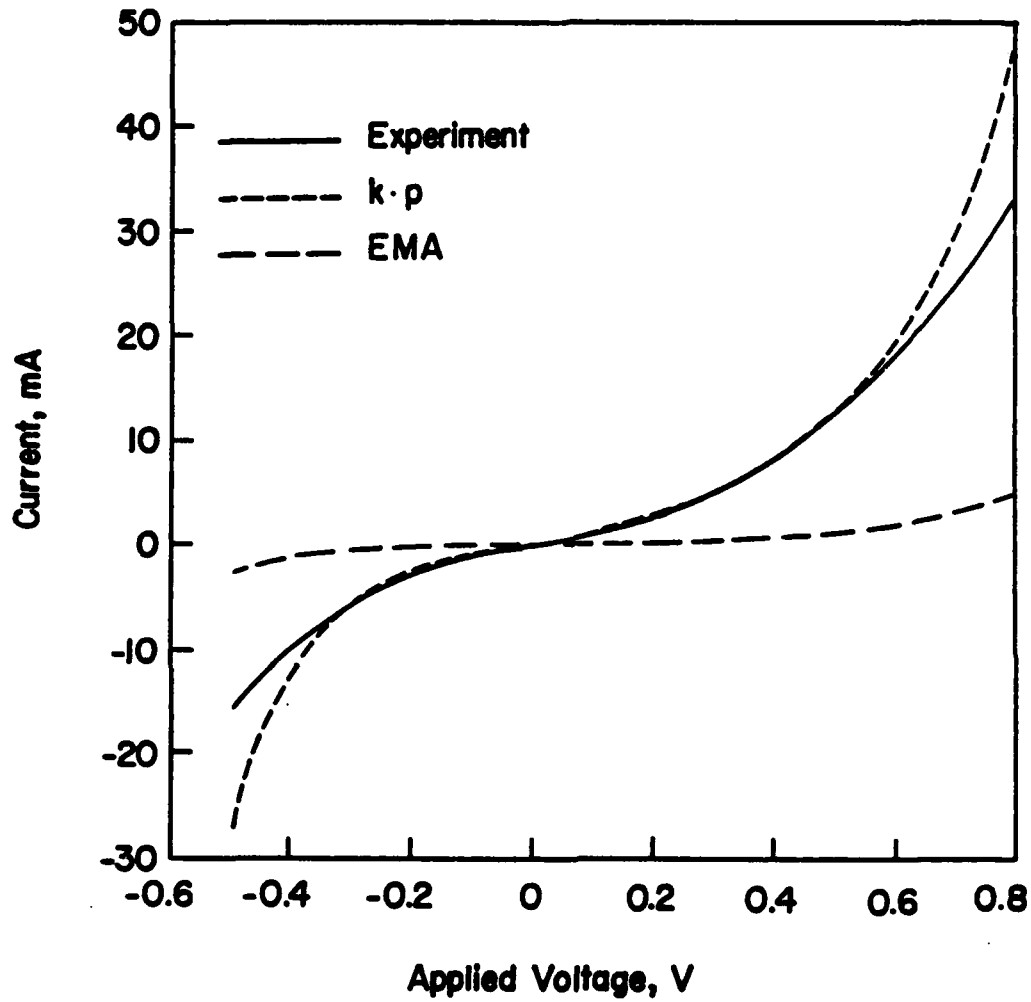


Fig. 10 Theoretical $k \cdot p$ (short dashed line) and effective-mass approximation (long dashed line), and experimental (solid line) I-V curves of the tunneling diode.

Publications/Presentations/Honors

a. Papers Submitted to Referred Journals

- C. J. Kiely, J. I. Chyi, A. A. Rockett, and H. Morkoç, "On the microstructure and interfacial structure of InSb layers grown on GaAs(100) by molecular beam epitaxy," *Phil. Mag. A*, in print. (MRL-DOE contract no. DE-AC02-76ER01198; AFOSR contract no. 86-0111; IBM)
- J. I. Chyi, D. Biswas, S. V. Iyer, N. S. Kumar, H. Morkoç, R. Bean, K. Zanio, H. Y. Lee, and H. Chen, "Molecular beam epitaxial growth and characterization of InSb on Si," *Appl. Phys. Lett.*, in print. (DOE)
- D. Mui, M. Patil, J. Chen, S. Agarwala, N. S. Kumar, and H. Morkoç, "Calculation of the I-V characteristics of direct tunneling diodes," *Solid State Electronics*, pending. (AFOSR)

b. Papers Published in Referred Journals

- D. Huang, J. Chyi, J. Klem, and H. Morkoç, "Optical properties of molecular beam epitaxially grown $\text{GaAs}_{1-x}\text{Sb}_x$ ($0 < x < 0.5$) on GaAs and InP substrates," *J. Appl. Phys.*, vol. 63, pp. 5859-5862, 1988.
- G. Ji, S. Agarwala, D. Huang, and H. Morkoç, "Band lineup in $\text{GaAs}_{1-x}\text{Sb}_x/\text{GaAs}$ strained-layer multiple quantum well grown by molecular beam epitaxy," *Phys. Rev. B*, vol. 38, pp. 10571-10577, 1988. (AFOSR; NASA; MRL-DOE contract no. DE-AC02-76ER01198)
- S. Kalem, J. Chyi, C. W. Litton, H. Morkoç, S. C. Kan, and A. Yariv, "Electrical properties of InAs epilayers grown by molecular beam epitaxy on Si substrates," *Appl. Phys. Lett.*, vol. 53, pp. 562-564, 1988. (AFOSR; AFOSR at CIT; ONR at CIT; NSF at CIT; ARO at CIT; SDIO-IST through JPL)
- J. I. Chyi, S. Kalem, N. S. Kumar, C. W. Litton, and H. Morkoç, "Growth of InSb and $\text{InAs}_{1-x}\text{Sb}_x$ on GaAs by molecular beam epitaxy," *Appl. Phys. Lett.*, vol. 53, pp. 1092-1094, 1988. (AFOSR)
- C. K. Peng, J. Chen, and H. Morkoç, "Contact regrowth technique for low-resistance nonalloyed contacts to the hot-electron transistor," *Appl. Phys. Lett.*, vol. 53, pp. 1738-1740, 1988. (NASA Lewis Research Center; AFOSR)

c. Books and Book Chapters Submitted for Publication

- H. Morkoç, H. Ünlü, and G. Ji, "Fundamentals and Technology of MODFETs," Wiley and Sons, pending. (AFOSR; NASA)

d. Books and Book Chapters Published

- H. Ünlü and H. Morkoç, "Growth and Properties of GaAs-Based Devices on Si," in *GaAs Technology*, Vol. II, Ed. D. K. Ferry, Howard Sons and Co., Indianapolis, 1988. (AFOSR)

h. Contributed Presentations at Scientific/Technical Society Conferences

- J. F. Klem, D. Huang, H. Morkoç, Y. E. Ihm, and N. Otsuka, "Optical characterization of $\text{GaAs}_{1-x}\text{Sb}_x$ and $\text{GaAs}_{1-x}\text{Sb}_x/\text{GaAs}$ strained layer superlattices," *Proceedings of the Society of Photo-Optical Instrumentation Engineers*, vol. 877, Los Angeles, CA, January 10-17, 1988, pp. 28-34. (NSF-MRL at Purdue University; DOE contract no. DE-AC04-76DP00789 at Sandia National Laboratories)

- J. Klem, J. I. Chyi, H. Morkoç, Y. E. Ihm, and N. Otsuka, "Electrical characteristics of MBE-grown $\text{GaAs}_{1-x}\text{Sb}_x$ on InP and correlation with film microstructure," *Proceedings of the Society of Photo-Optical Instrumentation Engineers*, vol. 877, Los Angeles, CA, January 10-17, 1988, pp. 35-40. (NSF-MRL at Purdue University; DOE contract no. DE-AC04-76DP00789 at Sandia National Laboratories)
- J. I. Chyi, S. Kalem, C. W. Litton, and H. Morkoç, "Growth and characterization of InSb and $\text{InAs}_{1-x}\text{Sb}_x$ grown on GaAs," presented at the Electronic Materials Conference, Boulder, CO, June 22-24, 1988.
- J. I. Chyi, D. Biswas, S. V. Iyer, N. S. Kumar, H. Morkoç, R. Bean, K. Zanio, R. Grober, and D. Drew, "MBE growth and characterization of InSb on Si," presented at the 9th MBE Workshop, West Lafayette, IN, Sept. 21-23, 1988. *J. Vac. Sci. Technol.*, in print.

i. Honors/Awards/Prizes

- Hadis Morkoç, Fellow, American Physical Society, for numerous innovative contributions in molecular beam epitaxial growth of semiconductor structures, 1988.
- David Sai Lai Mui, Fellowship, International Business Machines, 1988-89.

j. Graduate Students and Postdoctorals Supported Under the CRP for the Year Ending 1 October 1987

- James J. Chen
- Jen-Inn Chyi
- David S. L. Mui (AFOSR, IBM Fellowship)
- Chin-Kun Peng (AFOSR)
- Sambhu Agarwala (NASA)
- John F. Klem (DOE at Sandia National Laboratories)
- Dr. Seraf Kalem (AFOSR)